NANO LETTERS

pubs.acs.org/NanoLett Letter

Spectrum and Polarization-Resolved Nonlinear Optical Near-Field Imaging of Plasmonic Nanoantennas

Yaxin Liu, Jiajun Wang, Bingbing Zhu, Xinhao Wang, Sheng Zhang, Weifeng Liu, Lei Shi, and Zhensheng Tao*

Cite This: https://doi.org/10.1021/acs.nanolett.4c06081 Read Online

ACCESS | Metrics & More | Article Recommendations | Supporting Information

ABSTRACT: Plasmonic nanoantennas, which support surface plasmon resonances enabling the concentration of electromagnetic energy into subwavelength volumes, have emerged as versatile tools for a wide range of applications. However, achieving high-resolution near-field imaging with polarization and temporal sensitivity remains a significant challenge. In this work, we present a novel nonlinear optical microscopy technique based on degenerate four-wave mixing to enable spectrum- and polarization-resolved near-field imaging of plasmonic nanoantennas. By using a mid-infrared pump and near-infrared probe, we capture detailed spatial distributions of plasmon-enhanced near-field intensity and polarization characteristics, revealing distinct polarization patterns and frequency-dependent enhancements. Our method enables the observation of resonance-induced spectral shifts and subwavelength spatial resolution, offering valuable insights into plasmonic field behaviors, particularly in the mid-infrared range. This approach provides a powerful tool for exploring and understanding the complexities of plasmonic nanostructures, with significant potential for advancing nano-optics applications.

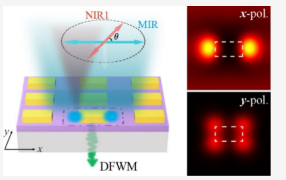

KEYWORDS: *plasmonic nanoantennas, near filed imaging, degenerate four-wave mixing, polarization-dependent signals, spectral modulation*

Plasmonic nanoantennas, typical made from metals such as gold (Au) and silver (Ag), have emerged as versatile tools in various research fields. These nanoantennas can support surface plasmon resonances, enabling the concentration of electromagnetic energy into subwavelength volumes, a phenomenon known as near-field enhancement.[1−3] This localized amplification of electromagnetic fields around plasmonic nanostructures has led to numerous applications in both linear and nonlinear optics, including biological sensing,[4−6] lasing,[7−10] light-matter interactions[11,12] second- and third-harmonic generation[13−18] and high-order harmonic generation.[19−22] To fully exploit the capabilities of plasmonic field enhancement, it is essential to probe the local near-fields, not only in terms of their amplitude but also their polarization and temporal characteristics.

Previously, scanning near-field optical microscopy (SNOM) has been employed to obtain valuable near-field information on plasmonic nanoantennas.[23−27] However, SNOM presents several limitations: fabricating sharp probing tips is technically challenging, and the close proximity of the SNOM tip to the sample surface can perturb local electromagnetic fields, leading to data artifacts.[28,29] In addition, energy-filtered electron energy-loss microscopy has been used to image the local near-fields of plasmonic structures.[30−32] However, the necessity for high-vacuum environments and thin samples greatly limits its broader application. Furthermore, both techniques encounter challenges in accurately capturing the polarization and phase information on plasmonic near-fields.

Alternatively, nonlinear optical responses of enhanced plasmonic near-fields with external probing pulses provide a promising approach for near-field imaging.[33−37] The polarization sensitivity inherent in nonlinear wave-mixing processes, along with spectral information, can offer comprehensive vectorial information about plasmonic near-fields. However, research in this area remains limited.

In this work, we demonstrate a novel imaging approach for plasmonic near-fields based on nonlinear optical microscopy, specifically focusing on degenerate four-wave mixing (DFWM) from silicon.[38] By employing a mid-infrared (MIR) pump and a near-infrared (NIR) probe, we achieve high-resolution polarization- and spectrum-resolved near-field imaging of Au nanoantennas. The spatial distribution of the plasmon-enhanced near-field intensity, as well as the in-plane polarization characteristics, are mapped in detail, revealing distinct polarization patterns. Our findings show frequency shifts in the DFWM emissions around the nanoantennas, attributed to frequency-dependent near-field enhancements. Furthermore, this approach enables the observation of resonance-induced spectral modulations and supports subwavelength spatial

Received: November 28, 2024
Revised: February 4, 2025
Accepted: February 4, 2025

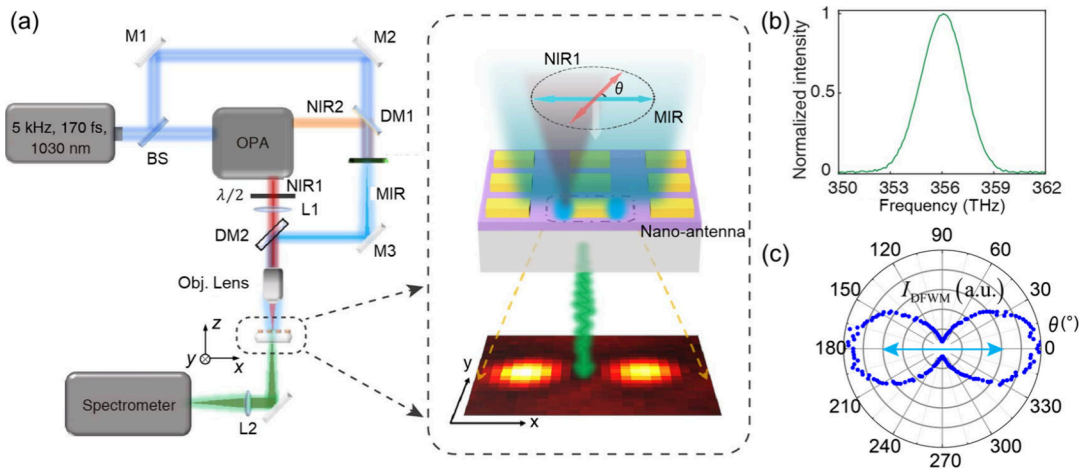

Figure 1. Experimental setup. (a) Schematic of the experimental setup. M: Mirror, BS: Beam splitter, OPA: Optical parametric amplifier, $\lambda/2$: Half waveplate, DM: Dichroic mirror, Obj. Lens: Objective lens, L: lens. (b) Spectrum of DFWM radiation. (c) DFWM intensity as a function of polarization angle θ, measured on a 140 nm thick silicon film excited by two linearly polarized beams. The MIR polarization is fixed at 0°, indicated by a blue double arrow, while θ represents the polarization angle of the NIR light.

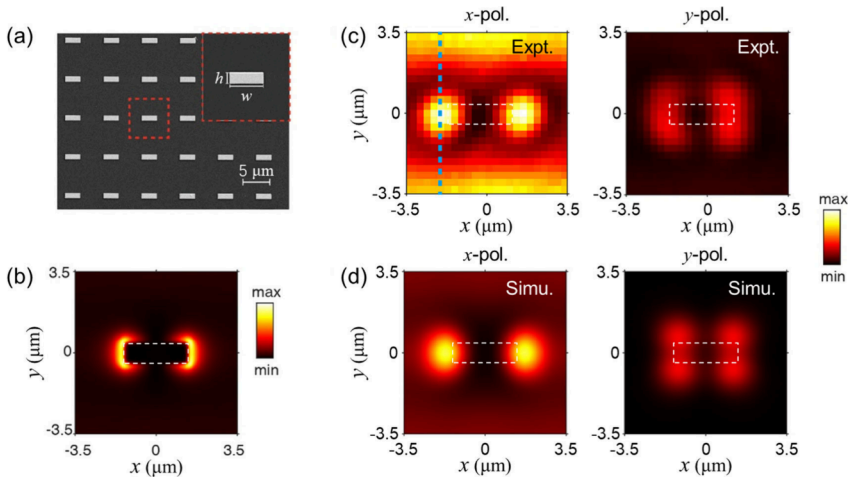

Figure 2. Polarization-resolved near-field imaging. (a) Scanning electron micrograph of the Au nanoantenna array. (b) Simulated near-field distribution around a single Au nanoantenna in the array. (c) Experimental (Expt.) imaging of the *x*-polarized (*x*-pol., left) and the *y*-polarized (*y*-pol., right) near-field components. Dashed line indicates the trajectory in Figure 3 and 4 below. (d) Same as (c) for the simulated (Simu.) near-field imaging. White boxes in (b–d) mark the outlines of the nanoantennas.

resolution, which is valuable for future plasmonic studies, particularly in the mid-infrared range.

Figure 1a illustrates the basic principle of our experiment. Plasmonic near-fields are resonantly excited by a MIR pump laser in an array of Au nanoantennas with a wavelength of $\lambda_{MIR} \approx 15$ μm (f_{MIR}= 23 THz). Simultaneously, the near-field distribution is probed by a NIR probe laser with a wavelength of $\lambda_{NIR} \approx 967$ nm (f_{NIR}= 310 THz). The nanoantenna array is fabricated on a silicon substrate using electron-beam lithography and evaporation (see Methods section for details of the sample preparation). In the experiment, the NIR probe beam is focused by an objective lens to a diameter of ~1 μm, much smaller than the wavelength of the MIR pump laser. The diameter of the MIR pump beam is ~30 μm to ensure homogeneous excitation of the near-field mode. Near-field imaging is realized by transversely scanning the sample with nanometer spatial resolution, while the spectra of the output beams are recorded by a spectrometer.

In our experiment, the excited MIR near-field penetrating into the silicon substrate is probed through the DFWM process in silicon, which involves nonlinear wave-mixing between the MIR local near-field ($\mathbf{E}^{NF}$) and the NIR probe field ($\mathbf{E}^{NIR}$). The nonlinear polarization associated with DFWM is described by

$$\mathbf{P}_{DFWM} = \varepsilon_0 \chi^{(3)} \cdot \mathbf{E}^{NIR} \cdot \mathbf{E}^{NF} \cdot \mathbf{E}^{NF} \quad (1)$$

where ε_0 is the vacuum permittivity, and $\chi^{(3)}$ represents the nonlinear susceptibility. The DFWM intensity (I_{DFWM}) is proportional to $|\mathbf{P}_{DFWM}|^2$while the frequency of the DFWM emission (f_{DFWM}) is given by

$$f_{DFWM} = f_{NIR} + 2 \times f_{NF} \quad (2)$$

where f_{NF} is the near-field frequency which corresponds to the MIR pump frequency f_{MIR}. A typical DFWM spectrum is shown in Figure 1b.

Since DFWM involves nonlinear wave-mixing in a dielectric material, the DFWM intensity (I_{DFWM}) depends on the polarization states in the *x*-*y* plane of the local near-fields and the NIR probe fields. The nonlinear polarization in eq 1

https://doi.org/10.1021/acs.nanolett.4c06081
Nano Lett. XXXX, XXX, XXX−XXX

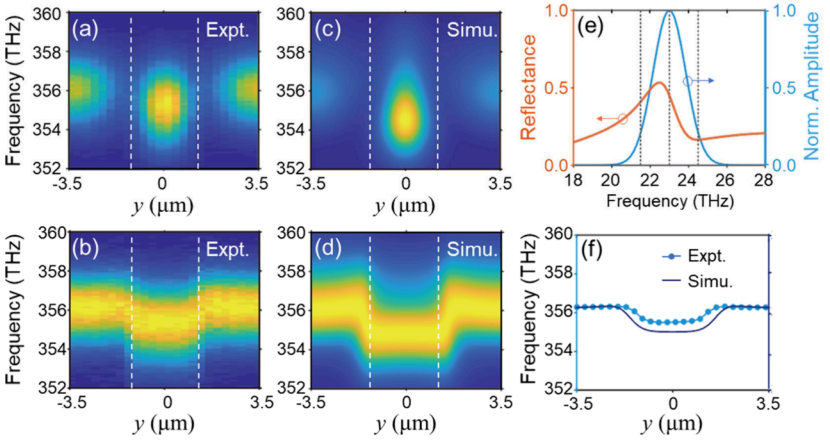

Figure 3. Spectrum-resolved near-field imaging. (a) Experimental DFWM intensity as a function of y along the trajectory shown in Figure 2c. Dashed lines indicate the positions where the frequency redshift occurs. (b) Experimental DFWM intensity normalized at each y value for the data shown in (a). (c) and (d) Same as (a) and (b), but for the simulated variation of the DFWM spectrum. (e) Simulated reflectance of the Au nanoantenna array (orange) and experimental amplitude of the pump MIR laser (blue). (f) DFWM center frequency as a function of y, obtained from the experimental and simulation results.

can be further expanded by considering different polarization components:

$$\begin{pmatrix} P_x \\ P_y \end{pmatrix} = \varepsilon_0 \chi^{(3)} \begin{pmatrix} 3E_x^{\mathrm{NIR}}(E_x^{\mathrm{NF}})^2 + 2E_y^{\mathrm{NIR}}E_x^{\mathrm{NF}}E_y^{\mathrm{NF}} + E_x^{\mathrm{NIR}}(E_y^{\mathrm{NF}})^2 \\ 3E_y^{\mathrm{NIR}}(E_y^{\mathrm{NF}})^2 + 2E_x^{\mathrm{NIR}}E_y^{\mathrm{NF}}E_x^{\mathrm{NF}} + E_y^{\mathrm{NIR}}(E_x^{\mathrm{NF}})^2 \end{pmatrix} \tag{3}$$

and the total DFWM intensity is given by $I_{\mathrm{DFWM}} \propto |P_x + P_y|^2$. Consequently, by aligning the probe-field polarization to the x or y axes, we can resolve different polarization components of the near-fields. This method is characterized by measuring the polarization-dependent I_{DFWM} on a silicon thin film with a thickness of 140 nm, which is excited by a homogeneous, linearly polarized MIR field (Figure 1c). The DFWM intensity reaches its maximum when the probe-field polarization aligns with the MIR field ($\theta = 0°$) and its minimum when it is perpendicular to the MIR field ($\theta = 90°$). The polarization extinction ratio is larger than 10.

We first demonstrate polarization-resolved near-field imaging of the plasmonic nanoantennas. In Figure 2a, we present the scanning electron micrograph of the array of Au nanoantennas. The length (w) of each antenna is 2.8 μm, and the width (h) is 0.95 μm, with its thickness being 90 nm. The period of the array is 7 μm. The nanoantenna array is designed to be on resonance at the MIR-laser frequency. According to the finite-difference time-domain (FDTD) simulations, the excited plasmonic near-fields in the silicon layer are localized and enhanced at the two ends of the Au nanoantennas when the MIR pump laser is polarized along the x axis (Figure 2b). In Figure 2c, we present the experimental measurements of the distribution of the x- and y-polarized near-fields, and the simulation results of the two polarization components are shown in Figure 2d. Our results indicate that the x-polarized near-fields dominantly distribute at the two ends of each nanoantenna, while the y-polarized fields are more localized at the four corners of the rectangular antenna. The distinct electric field patterns under different polarizations arise from the anisotropic geometry of the structure and the interaction between the incident field and the resonant plasmonic modes supported by the nanoantennas. Our simulation results are in excellent agreement with the experimental results, by taking the convolution of spatial resolution into account (see Supporting Information (SI)). In our experiment, the overall transverse resolution is about 1.35 μm, which is determined by the focal spot size of the NIR probe beam (~1 μm), the step size of the x-y displacement stage (0.3 μm), and the optical scattering properties of the samples.

The spectrum-resolving capability of our method further allows us to investigate the spectral response of plasmonic nanoantennas. In Figure 3a, we present the variation in the DFWM spectrum along the y-direction trajectory (the blue dashed line in Figure 2c). The DFWM intensity peaks at $y = 0$, indicating near-field enhancement near the Au nanoantenna. Along with the intensity modulation, Figure 3b exhibits a central-frequency shift in the DFWM spectrum along the same trajectory, where spectral redshifts are observed in the same enhancement region. In Figure 3c,d, we present the FDTD simulation results for the intensity and frequency variations, respectively. In the simulation, a MIR-pump beam with a central frequency of f_{MIR} = 22.5 THz is incident on the nanoantennas, with its polarization aligned along the x direction, and a reflectance peak is observed around f_{MIR}. The DFWM spectrum is further simulated using eq 2, incorporating the near-field distribution around the nanoantennas. The simulation results can well capture the observed intensity modulation and frequency redshifts (Figure 3c,d).

The spectral redshifts can be explained by the frequency-dependent enhancement of the near-fields. Figure 3e presents the resonant spectral response of the Au nanoantenna array, which peaks around 22.5 THz. The central frequency of the MIR pulse is approximately 23 THz, slightly offset from the peak and positioned at the higher-frequency edge of the resonant curve (Figure 3e). Consequently, the nanoantenna array enhances the lower-frequency portion of the incident MIR pulse, leading to the observed redshifts in the DFWM spectrum. In Figure 3f, we extract the central frequencies of the experimental and simulation results, and excellent agreement can be realized.

The ability to resolve the near-field spectral response of nanoplasmonics opens up new possibility of assessing the local temporal waveforms of plasmonic fields. The spectral information is directly extracted from the experimental results,

https://doi.org/10.1021/acs.nanolett.4c06081
Nano Lett. XXXX, XXX, XXX−XXX

while we resort to simulations for the phase information. In Figure 4a, we present the simulated near-field waveforms along

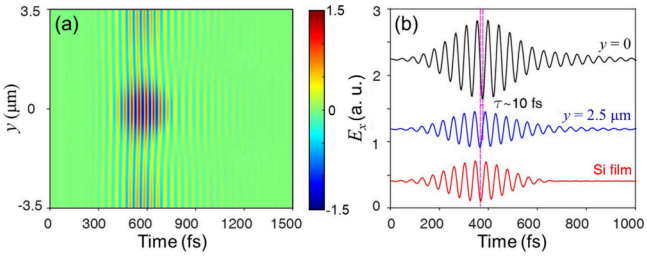

Figure 4. Temporal traces of near-fields around the Au nanoantenna. (a) Simulated temporal traces of the near-fields around the Au nanoantenna along the trajectory shown in Figure 2c. (b) Extracted temporal traces at the center of near-field resonance (y = 0), in the off-resonance area (y = 2.5 μm), and on a silicon thin film. A time shift of ∼10 fs is labeled between the on-resonance and off-resonance traces.

the y-line across a unit cell of the Au nanoantenna array (see Figure 2c). In addition to near-field enhancement, phase shifts in the near-field waveforms can be observed. Figure 4b shows the extracted waveforms at three positions: on-resonance at y = 0, off-resonance at y = 2.5 μm, and on a silicon thin film. The enhanced near-field away from the Au nanoantennas exhibits a similar temporal profile compared to the near-field on the silicon film. The near-field located at the nanoantenna resonance is about 10 fs delayed compared to the field away from Au nanoantennas and the Si film, which can be understood from the near-filed phase modulations in the frequency domain (see SI Section 7). The near-field phase can be experimentally measured through quantum-path interference between neighboring harmonic orders,[39−41] enabling future reconstruction of plasmonic near-field waveforms.

In conclusion, our study presents a powerful method for investigating the near-field characteristics of plasmonic nanoantennas using nonlinear optical microscopy. The experimental setup allows detailed mapping of the near-field intensity and polarization distributions, uncovering frequency-dependent behaviors and resonance-induced spectral shifts. The subwavelength resolution achieved with this technique offers valuable insights into plasmonic field enhancements and demonstrates potential for advanced applications in mid-infrared nano-optics. This approach contributes a robust tool for plasmonic research, providing a new pathway for near-field imaging in complex nanostructures.

METHODS

Sample Fabrication. The Au nanoantennas were fabricated on a 500 μm-thick optical glass substrate. A 140 nm-thick silicon film was first deposited on the substrate by magnetron sputtering. A 300 nm-thick layer of CSAR 62 positive electron beam resist was then spin-coated, followed by an additional layer of conductive polymer (AR-PC 5092.02). The nanoantenna patterns were prefabricated onto the photoresist layer using electron beam lithography (EBL) (ZEISS Sigma 300), which served as a mask for the subsequent processes. A 1 nm-thick Cr adhesive layer and a 90 nm-thick Au layer were then deposited onto the EBL-patterned photoresist using electron beam evaporation. The final Au nanoantennas were obtained through a standard lift-off process.

Numerical Simulations. The numerical simulations were performed with the commercial software Lumerical FDTD Solutions. Bloch boundary conditions were applied in the x and y directions, while perfect matching layers (PML) was applied in the z direction. The plane-wave type was set as BFAST. A plane-wave pulse source being x-polarized (parallel to the long side of Au nanoantennas) was set normally incident onto the structure from the air side.

For the reflectance simulation in Figure 3e and the frequency-dependent electric field intensity simulation in Figure S2, the source was defined in the frequency domain, with the wavelength range set from 6 to 20 μm. For the simulation results shown in Figures 2b,d and 3c,d and Figure S1, the source was set in the time domain to match the experimental pump pulse conditions. In these cases, the center frequency was set to 23 THz and the pulse duration was 200 fs. To capture both the time-dependent features of the pump excitation and frequency-dependent modulations, frequency-domain power monitors and time monitors were used in the simulations.

Experimental Setup. The experimental setup was based on an Yb: KGW laser system, delivering laser pulses of 170 fs duration with a central wavelength of 1030 nm and a repetition rate of 5 kHz. As shown in Figure 1a, the laser is first split into two parts by a beam splitter (BS): input 1 and input 2. Input 1 enters an optical parametric amplifier (OPA) system, where two light pulses can be generated: One is the NIR light (NIR1, about 310 THz) used to excite the DFWM emission (red light beam in Figure 1a), and the other is tunable NIR light (NIR2) (orange light beam in Figure 1a). For the measurement, the center frequency of NIR2 was set to about 268 THz.

The input 2 and NIR2 were combined by a dichroic mirror (DM1), and difference frequency generation (DFG) in a GaSe crystal produces the MIR light used for the measurements. A second dichroic mirror (DM2) was applied to combine the NIR1 and MIR light. The two light pulses are colinearly focused onto the sample using an objective lens. The diameter of the focused NIR1 spot is approximately 1 μm, while the focused MIR spot has a diameter of about 30 μm. Since the focused NIR1 spot is smaller than the wavelength of the MIR light, subwavelength resolution in the MIR range is achieved. The DFWM emissions are collected by a spectrometer, allowing for the measurement of spectral dependencies.

The sample is mounted on an XYZ displacement stage, enabling two-dimensional imaging by adjusting the relative position between the sample and the focused excitation beams. Additionally, a half-wave plate ($\lambda/2$) is used to adjust the polarization of NIR2. Using this DFWM-sweep imaging system, both spatial and spectral distributions can be measured.

ASSOCIATED CONTENT

Supporting Information

The Supporting Information is available free of charge at https://pubs.acs.org/doi/10.1021/acs.nanolett.4c06081.

Processing for the simulation results, near-field enhancement variation at different frequencies, spectral distribution along the x direction, demonstration of the intensity dependence, measurement of reflection spectra, and simulated resonance-induced phase modulations in the frequency domain (PDF)

https://doi.org/10.1021/acs.nanolett.4c06081
Nano Lett. XXXX, XXX, XXX−XXX

AUTHOR INFORMATION

Corresponding Author

Zhensheng Tao − *State Key Laboratory of Surface Physics and Key Laboratory of Micro and Nano Photonic Structures (MOE), Department of Physics, Fudan University, Shanghai 200433, P. R. China; Shanghai Key Laboratory of Metasurfaces for Light Manipulation, Fudan University, Shanghai 200433, P. R. China;* orcid.org/0000-0002-8727-3719; Email: zhenshengtao@fudan.edu.cn

Authors

Yaxin Liu − *State Key Laboratory of Surface Physics and Key Laboratory of Micro and Nano Photonic Structures (MOE), Department of Physics, Fudan University, Shanghai 200433, P. R. China; Shanghai Key Laboratory of Metasurfaces for Light Manipulation, Fudan University, Shanghai 200433, P. R. China;* orcid.org/0000-0002-2674-7634

Jiajun Wang − *State Key Laboratory of Surface Physics and Key Laboratory of Micro and Nano Photonic Structures (MOE), Department of Physics, Fudan University, Shanghai 200433, P. R. China; Shanghai Key Laboratory of Metasurfaces for Light Manipulation, Fudan University, Shanghai 200433, P. R. China*

Bingbing Zhu − *State Key Laboratory of Surface Physics and Key Laboratory of Micro and Nano Photonic Structures (MOE), Department of Physics, Fudan University, Shanghai 200433, P. R. China; Shanghai Key Laboratory of Metasurfaces for Light Manipulation, Fudan University, Shanghai 200433, P. R. China*

Xinhao Wang − *State Key Laboratory of Surface Physics and Key Laboratory of Micro and Nano Photonic Structures (MOE), Department of Physics, Fudan University, Shanghai 200433, P. R. China; Shanghai Key Laboratory of Metasurfaces for Light Manipulation, Fudan University, Shanghai 200433, P. R. China*

Sheng Zhang − *State Key Laboratory of Surface Physics and Key Laboratory of Micro and Nano Photonic Structures (MOE), Department of Physics, Fudan University, Shanghai 200433, P. R. China; Shanghai Key Laboratory of Metasurfaces for Light Manipulation, Fudan University, Shanghai 200433, P. R. China*

Weifeng Liu − *State Key Laboratory of Surface Physics and Key Laboratory of Micro and Nano Photonic Structures (MOE), Department of Physics, Fudan University, Shanghai 200433, P. R. China; Shanghai Key Laboratory of Metasurfaces for Light Manipulation, Fudan University, Shanghai 200433, P. R. China*

Lei Shi − *State Key Laboratory of Surface Physics and Key Laboratory of Micro and Nano Photonic Structures (MOE), Department of Physics, Fudan University, Shanghai 200433, P. R. China; Shanghai Key Laboratory of Metasurfaces for Light Manipulation, Fudan University, Shanghai 200433, P. R. China*

Complete contact information is available at: https://pubs.acs.org/10.1021/acs.nanolett.4c06081

Author Contributions

Y.L. and J.W. contributed equally to this work.

Notes

The authors declare no competing financial interest.

ACKNOWLEDGMENTS

This work was accomplished in Fudan University. We wish thank Jiasheng Zhang for technical support. Z.T. acknowledges the support from the National Key Research and Development Program of China (Grant No. 2021YFA1400200, 2022YFA1404700). Z.T. and L.S. both acknowledge the support from the National Natural Science Foundation of China (No. 12221004). We also acknowledge the support from the National Natural Science Foundation of China (Nos. 12274091, 62192771, T2394480, T2394481, 12234007, 12321161645 and 12404427), the National Key R&D Program of China (Nos. 2022YFA1404800 and 2023YFA1406900), and the Shanghai Municipal Science and Technology (Grant Nos. 22JC1400200, 22142200400, 21DZ1101500, 2019SHZDZX01, 23DZ2260100, and 24YF2702400). J.W. also acknowledges the support from the China National Postdoctoral Program for Innovative Talents (BX20230079) and the China Postdoctoral Science Foundation (2023M740721).

REFERENCES

(1) Klar, T.; Perner, M.; Grosse, S.; Von Plessen, G.; Spirkl, W.; Feldmann, J. Surface-Plasmon Resonances in Single Metallic Nanoparticles. *Phys. Rev. Lett.* **1998**, *80*, 4249.

(2) Ciracì, C.; Hill, R. T.; Mock, J. J.; Urzhumov, Y.; Fernández-Domínguez, A. I.; Maier, S. A.; Pendry, J. B.; Chilkoti, A.; Smith, D. R. Probing the Ultimate Limits of Plasmonic Enhancement. *Science (80-.)* **2012**, *337*, 1072−1074.

(3) Krasnok, A.; Tymchenko, M.; Alù, A. Nonlinear Metasurfaces: A Paradigm Shift in Nonlinear Optics. *Mater. Today* **2018**, *21*, 8−21.

(4) Wang, M.; Wang, T.; Ojambati, O. S.; Duffin, T. J.; Kang, K.; Lee, T.; Scheer, E.; Xiang, D.; Nijhuis, C. A. Plasmonic Phenomena in Molecular Junctions: Principles and Applications. *Nat. Rev. Chem.* **2022**, *6*, 681−704.

(5) Anker, J. N.; Hall, W. P.; Lyandres, O.; Shah, N. C.; Zhao, J.; Van Duyne, R. P. Biosensing with Plasmonic Nanosensors. *Nat. Mater.* **2008**, *7*, 442−453.

(6) Höppener, C.; Novotny, L. Antenna-Based Optical Imaging of Single Ca2+ Transmembrane Proteins in Liquids. *Nano Lett.* **2008**, *8*, 642−646.

(7) Taskinen, J. M.; Moilanen, A. J.; Rekola, H.; Kuntze, K.; Priimagi, A.; Törmä, P.; Hakala, T. K. All-Optical Emission Control and Lasing in Plasmonic Lattices. *ACS Photonics* **2020**, *7*, 2850−2858.

(8) Salerno, G.; Heilmann, R.; Arjas, K.; Aronen, K.; Martikainen, J.-P.; Törmä, P. Loss-Driven Topological Transitions in Lasing. *Phys. Rev. Lett.* **2022**, *129*, 173901.

(9) Deng, S.; Li, R.; Park, J.-E.; Guan, J.; Choo, P.; Hu, J.; Smeets, P. J. M.; Odom, T. W. Ultranarrow Plasmon Resonances from Annealed Nanoparticle Lattices. *Proc. Natl. Acad. Sci. U. S. A.* **2020**, *117*, 23380−23384.

(10) Fernandez-Bravo, A.; Wang, D.; Barnard, E. S.; Teitelboim, A.; Tajon, C.; Guan, J.; Schatz, G. C.; Cohen, B. E.; Chan, E. M.; Schuck, P. J.; et al. Ultralow-Threshold, Continuous-Wave Upconverting Lasing from Subwavelength Plasmons. *Nat. Mater.* **2019**, *18*, 1172−1176.

(11) You, B.; Du, Y.; Yuan, S.; Tian, Y.; Meng, X.; Wu, W.; Shi, Z.; Wang, G.; Chen, X.; Yuan, X.; Zhu, X. Strong Coupling between Moiré-Type Plasmons and Phonons in Suspended Monolayer Metallic Twisted Superlattices. *Nano Lett.* **2024**, *24*, 15837−15844.

(12) Li, Y.; Hu, H.; Jiang, W.; Shi, J.; Halas, N. J.; Nordlander, P.; Zhang, S.; Xu, H. Duplicating Plasmonic Hotspots by Matched Nanoantenna Pairs for Remote Nanogap Enhanced Spectroscopy. *Nano Lett.* **2020**, *20*, 3499−3505.

(13) Zhang, C. C.; Zhang, J. Y.; Feng, J. R.; Liu, S. T.; Ding, S. J.; Ma, L.; Wang, Q. Q. Plasmon-Enhanced Second Harmonic

Generation of Metal Nanostructures. *Nanoscale* **2024**, *16*, 5960−5975.
(14) Deng, J.; Tang, Y.; Chen, S.; Li, K.; Zayats, A. V.; Li, G. Giant Enhancement of Second-Order Nonlinearity of Epsilon-near- Zero Medium by a Plasmonic Metasurface. *Nano Lett.* **2020**, *20*, 5421−5427.
(15) Gürdal, E.; Horneber, A.; Meixner, A. J.; Kern, D. P.; Zhang, D.; Fleischer, M. Enhancement of the Second Harmonic Signal of Nonlinear Crystals by a Single Metal Nanoantenna. *Nanoscale* **2020**, *12*, 23105−23115.
(16) Metzger, B.; Gui, L.; Fuchs, J.; Floess, D.; Hentschel, M.; Giessen, H. Strong Enhancement of Second Harmonic Emission by Plasmonic Resonances at the Second Harmonic Wavelength. *Nano Lett.* **2015**, *15*, 3917−3922.
(17) Jeong, T. I.; Oh, D. K.; Kim, S.; Park, J.; Kim, Y.; Mun, J.; Kim, K.; Chew, S. H.; Rho, J.; Kim, S. Deterministic Nanoantenna Array Design for Stable Plasmon-Enhanced Harmonic Generation. *Nanophotonics* **2023**, *12*, 619−629.
(18) Hanke, T.; Krauss, G.; Träutlein, D.; Wild, B.; Bratschitsch, R.; Leitenstorfer, A. Efficient Nonlinear Light Emission of Single Gold Optical Antennas Driven by Few-Cycle near-Infrared Pulses. *Phys. Rev. Lett.* **2009**, *103*, 1−4.
(19) Han, S.; Kim, H.; Kim, Y. W.; Kim, Y. J.; Kim, S.; Park, I. Y.; Kim, S. W. High-Harmonic Generation by Field Enhanced Femtosecond Pulses in Metal-Sapphire Nanostructure. *Nat. Commun.* **2016**, *7*, 1−7.
(20) Sivis, M.; Duwe, M.; Abel, B.; Ropers, C. Extreme-Ultraviolet Light Generation in Plasmonic Nanostructures. *Nat. Phys.* **2013**, *9*, 304−309.
(21) Vampa, G.; Ghamsari, B. G.; Siadat Mousavi, S.; Hammond, T. J.; Olivieri, A.; Lisicka-Skrek, E.; Naumov, A. Y.; Villeneuve, D. M.; Staudte, A.; Berini, P.; Corkum, P. B. Plasmon-Enhanced High-Harmonic Generation from Silicon. *Nat. Phys.* **2017**, *13*, 659−662.
(22) Genevet, P.; Tetienne, J. P.; Gatzogiannis, E.; Blanchard, R.; Kats, M. A.; Scully, M. O.; Capasso, F. Large Enhancement of Nonlinear Optical Phenomena by Plasmonic Nanocavity Gratings. *Nano Lett.* **2010**, *10*, 4880−4883.
(23) Wang, L.; Xu, X. G. Scattering-Type Scanning near-Field Optical Microscopy with Reconstruction of Vertical Interaction. *Nat. Commun.* **2015**, *6*, 1−9.
(24) Chen, X.; Hu, D.; Mescall, R.; You, G.; Basov, D. N.; Dai, Q.; Liu, M. Modern Scattering-Type Scanning Near-Field Optical Microscopy for Advanced Material Research. *Adv. Mater.* **2019**, *31*, 1−24.
(25) Ma, X.; Liu, Q.; Yu, N.; Xu, D.; Kim, S.; Liu, Z.; Jiang, K.; Wong, B. M.; Yan, R.; Liu, M. 6 Nm Super-Resolution Optical Transmission and Scattering Spectroscopic Imaging of Carbon Nanotubes Using a Nanometer-Scale White Light Source. *Nat. Commun.* **2021**, *12*, 1−7.
(26) Denkova, D.; Verellen, N.; Silhanek, A. V.; Valev, V. K.; Dorpe, P. V.; Moshchalkov, V. V. Mapping Magnetic Near-Field Distributions of Plasmonic Nanoantennas. *ACS Nano* **2013**, *7*, 3168−3176.
(27) Neuman, T.; Alonso-González, P.; Garcia-Etxarri, A.; Schnell, M.; Hillenbrand, R.; Aizpurua, J. Mapping the near Fields of Plasmonic Nanoantennas by Scattering-type Scanning Near-field Optical Microscopy. *Laser Photon. Rev.* **2015**, *9*, 637−649.
(28) Moon, K.; Park, H.; Kim, J.; Do, Y.; Lee, S.; Lee, G.; Kang, H.; Kim, J. W.; Han, H. Subsurface Nanoimaging by THz Pulse Near-Field Microscopy. *Nano Lett.* **2015**, *15*, 549−552.
(29) Rotenberg, N.; Kuipers, L. Mapping Nanoscale Light Fields. *Nat. Photonics* **2014**, *8*, 919−926.
(30) Polman, A.; Kociak, M.; García de Abajo, F. J. Electron-Beam Spectroscopy for Nanophotonics. *Nat. Mater.* **2019**, *18*, 1158−1171.
(31) Nelayah, J.; Kociak, M.; Stéphan, O.; De Abajo, F. J. G.; Tencé, M.; Henrard, L.; Taverna, D.; Pastoriza-Santos, I.; Liz-Marzán, L. M.; Colliex, C. Mapping Surface Plasmons on a Single Metallic Nanoparticle. *Nat. Phys.* **2007**, *3*, 348−353.
(32) Piazza, L.; Lummen, T. T. A.; Quiñonez, E.; Murooka, Y.; Reed, B. W.; Barwick, B.; Carbone, F. Simultaneous Observation of the Quantization and the Interference Pattern of a Plasmonic Near-Field. *Nat. Commun.* **2015**, *6*, 6407.
(33) Constant, T. J.; Hornett, S. M.; Chang, D. E.; Hendry, E. All-Optical Generation of Surface Plasmons in Graphene. *Nat. Phys.* **2016**, *12*, 124−127.
(34) Harutyunyan, H.; Palomba, S.; Renger, J.; Quidant, R.; Novotny, L. Nonlinear Dark-Field Microscopy. *Nano Lett.* **2010**, *10*, 5076−5079.
(35) Blechman, Y.; Almeida, E.; Sain, B.; Prior, Y. Optimizing the Nonlinear Optical Response of Plasmonic Metasurfaces. *Nano Lett.* **2019**, *19*, 261−268.
(36) Schust, J.; Mangold, F.; Sterl, F.; Metz, N.; Schumacher, T.; Lippitz, M.; Hentschel, M.; Giessen, H. Spatially Resolved Nonlinear Plasmonics. *Nano Lett.* **2023**, *23*, 5141−5147.
(37) Alam, M. Z.; Schulz, S. A.; Upham, J.; De Leon, I.; Boyd, R. W. Large Optical Nonlinearity of Nanoantennas Coupled to an Epsilon-near-Zero Material. *Nat. Photonics* **2018**, *12*, 79−83.
(38) Boyd, R. W.; Gaeta, A. L.; Giese, E. Nonlinear Optics. In *Springer Handbook of Atomic, Molecular, and Optical Physics*; Springer: 2008; pp 1097−1110.
(39) Zhu, B.; Cai, Q.; Liu, Y.; Zhang, S.; Liu, W.; He, Q.; Zhou, L.; Tao, Z. Super-Resolution 3D Tomography of Vector near-Fields in Dielectric Resonators. arXiv Prepr. arXiv2406.13171, 2024.
(40) Liu, Y.; Jiang, S.; Zhu, B.; Zhang, S.; Liu, W.; Tao, Z. Investigation of Spectro-Temporal High-Order Sideband Generation from Transition Metal Dichalcogenides. *JOSA B* **2024**, *41*, B32−B39.
(41) Liu, Y.; Zhu, B.; Jiang, S.; Huang, S.; Luo, M.; Zhang, S.; Yan, H.; Zhang, Y.; Lu, R.; Tao, Z. Dephasing of Strong-Field-Driven Excitonic Autler-Townes Doublets Revealed by Time-and Spectrum-Resolved Quantum-Path Interferometry. *Phys. Rev. Lett.* **2024**, *133*, 26901.

https://doi.org/10.1021/acs.nanolett.4c06081
Nano Lett. XXXX, XXX, XXX−XXX